

Article

Machining GX2CrNiMoN26-7-4 DSS Alloy: Wear Analysis of TiAlN and TiCN/Al₂O₃/TiN Coated Carbide Tools Behavior in Rough End Milling Operations

Francisco José Gomes Silva *, Rui Pedro Martinho, Carlos Martins, Hernâni Lopes
and Ronny Miguel Gouveia

ISEP—School of Engineering, Polytechnic Institute of Porto, 4249-015 Porto, Portugal; rpm@isep.ipp.pt (R.P.M.); 1130062@isep.ipp.pt (C.M.); hml@isep.ipp.pt (H.L.); ronnygouveia@gmail.com (R.M.G.)

* Correspondence: fgs@isep.ipp.pt; Tel.: +351-228340500

Received: 4 May 2019; Accepted: 14 June 2019; Published: 17 June 2019



Abstract: In the last decade, it has been common to observe a competition between coatings achieved via physical vapor deposition (PVD) and chemical vapor deposition (CVD) techniques on cutting tools used in machining processes. The tool's substrate material can immediately condition the coating process selection. However, there are also materials capable of adapting to any of the coating processes. Hence, the capabilities demonstrated by a given coating when created with one technique or another are usually different due to the intrinsic characteristics of each coating process, such as temperature and stress levels. In this work, to study the machining behavior of a super duplex stainless steel, PVD- and CVD-coated tungsten carbide inserts with different coatings were used in order to identify the wear mechanisms that affect each of the coatings and the workpiece's surface quality, evaluated through different roughness parameters. The vibration level produced throughout the various tests was also registered in an attempt to associate the type of coating or insert failure with the level of vibrations generated in the CNC (Computer Numeric Control) machining spindle. This allowed us to conclude that the tools coated with TiAlN via PVD showed better wear behavior, as well as creating workpiece surfaces with less roughness. Thus, it was clear that this coating presents strong advantages in the machining of the super duplex stainless steel chosen for this work, being an innovative work due to the combination of materials used and the approach in terms of vibration analysis applied to milling.

Keywords: cutting tools; CVD; PVD; coatings; wear behavior; duplex stainless steel; surface roughness; vibration analysis

1. Introduction

Plasma coating deposition and synthesis techniques have evolved significantly in recent decades, currently with very high levels of sophistication, both through single-layer coatings, multi-layer coatings, and coatings that evolve from a material or composite on one surface, to another on the opposite surface of the coating, gradually passing from one material to another. These techniques have been deeply studied through different and recent overviews which explain their fundamentals and how they have evolved in recent years [1–3]. In order to increase tool lifespan and boost productivity, carbide and nitride tools have been gaining more and more market share, with tungsten carbide being used very frequently. In addition to further snowballing the lifespan of tools and subjecting them to increasingly severe working conditions, inserts are further coated with the above-mentioned plasma techniques [4,5]. At the outset, the chemical vapor deposition (CVD) technique was heavily

exploited in obtaining diamond coatings [6,7], but evolved into many other materials as diamond is not suitable for machining ferrous alloys. Currently, CVD diamond-coated tools are frequently used in the machining of composites and non-ferrous alloys [8,9]. On the other hand, physical vapor deposition (PVD) has been used with numerous materials and in diverse applications [10–12], including inserts for machining. Recently, in order to delimit the conditions of use of tools coated with both PVD and CVD, Boing et al. [13] conducted a study to investigate tool behavior when machining three different hardened steels, namely AISI 4340, AISI 52100 and AISI D2. Cutting parameters were set to those usually used when machining with PCBN inserts, to allow a tool cutting capacity for a minimum of 15 min. After coating degradation, the edge of the insert collapses, also observing that the TiAlN coating deposited via PVD is best suited to machine AISI 4340 (55 HRC) steel, while TiCN/Al₂O₃/TiN coatings made via CVD present a greater lifespan when machining AISI 52100 and D2 steels (50 and 45 HRC, respectively). A study carried out by Chinchankar and Choudhury [14] based on turning operations in AISI 4340 steel with 35 HRC hardness and using uncoated tools, PVD TiAlN mono-layered coated tools and CVD multi-layered TiCN/Al₂O₃/TiN coated tools, showed it is possible to increase cutting speeds from 62 m/min to about 200 m/min with PVD coated tools with a single layer of TiAlN and from 300 to 350 m/min in the case of tools provided with a multi-layered coating performed via CVD. The wear phenomena observed were essentially flank wear, crater wear, and catastrophic failure; it was found that cutting forces grow rapidly when the film is no longer present on the substrate. The authors also verified that tool lifespan is strongly affected by the selected cutting speed, mainly in the cases of uncoated tools and PVD mono-layered TiAlN coated tools. Also, CVD multi-layer coated tools present a longer lifespan than the PVD coated ones, essentially due to the greater thickness of the CVD coating. The wear of the TiAlN mono-layer obtained by PVD is slow but, when the coating fails, the tool degrades very easily by crater wear. A similar study carried out more recently by the same authors (Chinchankar and Choudhury) [15], also based on AISI 4340 turning operations, concluded that the forces developed during machining increased the higher the steel hardness, when using TiCN/Al₂O₃/TiN CVD coatings. On the other hand, the best surface quality was obtained with the higher hardness AISI 4340 steel when using a single-layer coating of TiAlN produced via PVD technique. In this case, the CVD coated carbide tools had a longer lifespan, which was also due to the greater thickness of the CVD coating (2 µm for the PVD coating and 18 µm for the CVD coating), as well as the existing Al₂O₃ layer, which protects the tool from the intense abrasive process at such high temperatures. The same steel (AISI 4340) was also studied by Kene et al. [16] in turning operations with TiAlN carbide multi-layered coated tools, verifying that the use of multi-layers presents economic advantages (in comparison to the same coating applied in mono-layered form) in terms of the tool's lifespan, as well as better workpiece surface finish and greater dimensional accuracy. Navas and Bengoetxea [17] also studied the machining process of AISI 4340 steel using uncoated tools and CVD coated tools, concluding that CVD coated tools lead to better surface quality and less residual stresses. Choudhury et al. [18] recently tested TiB₂ PVD coated carbide tools in rough turning operations of Ti6Al4V alloys, noting that the lifespan of this tool had a 70% increase when compared to an identical tool substrate coated with TiAlN, despite the strong built up edge (BUE) formation on the tool's edge surface during the chip forming process. Martinez et al. [19] studied the turning process of some metallic alloys such as AISI 1045 steel, AISI 4135 steel, Ductile Cast Iron, and Inconel 718 with TiN- and TiAlN PVD-coated carbide tools, stating that when analyzing flank wear and cutting distance, the relation between them fits a log–log scale plot. Moreover, the coating begins to wear progressively until it is completely detached, leaving the substrate as the sole supporter of wear progression, whereby its progression depends on the quality of the carbide grade used. Using the Taguchi methodology, Debnath et al. [20] performed a study based on turning operations of soft steel with a hardness of 130 BHN using carbide inserts coated with TiCN/Al₂O₃/TiN obtained via CVD, in order to identify the best set of parameters to be used. In this study, it was verified that the factor that most strongly affects the surface roughness is feed rate, while the cutting speed affects the wear rate more significantly.

Duplex stainless steels (DSS) are very particular alloys within the group of stainless steels, which have very balanced microstructural amounts of ferrite and austenite phases, allowing them to exhibit fairly attractive properties such as mechanical strength and corrosion resistance [21]. When the ratio between the contents of these two phases approaches 1, the best conjugation between mechanical properties and corrosion resistance properties is obtained [22,23]. The excellence of these properties comes from the high chromium content that these alloys contain, as well as small but very useful Molybdenum and nitrogen contents [24], which can be improved and of use when an outstanding pitting resistance equivalent number is required [25]. Due to the interest in the combination of these two important properties, these alloys have as preferred applications the petrochemical and chemical industries, nuclear power generators, water desalination stations, marine infrastructures, paper industry, heat exchangers, among many others [26,27]. However, some properties, which are very appreciated regarding the applications for which they are intended, have adverse consequences concerning their processing, for example, in machining. In fact, the high tenacity presented by these alloys, high work hardening effect, low thermal conductivity, and strong tendency for the formation BUE, make processing these materials through chip-cutting machining difficult. In fact, the work hardening effect promotes friction between the cutting edge of the tool and the workpiece, constituting an additional source of heat in this area, inducing oxidation and diffusion phenomena [28,29]. On the other hand, persistent BUE formation and adhesive wear occur essentially due to the chemical/metallurgical affinity between the tool's material and the duplex stainless steel being machined, usually resulting in continuous chip formation, which is undesirable [30,31]. Furthermore, the low thermal conductivity presented by these alloys limits the flow of heat generated at the cutting edge and adjacent zones, creating high temperature peaks, which contribute to a faster degradation of cutting capacity. A comparative study of three different types of stainless steel, namely AISI 316L, SAF 2205, and SAF 2507, revealed that the AISI 316L austenitic stainless steel is the easiest to cut, observing as well higher BUE formation on tool cutting edges as the workpiece's Cr and Mo content increases [32]. One study regarding the end milling of a SAF 2507 alloy was carried maintaining either a fixed feed-rate or cutting speed and varying the other parameter. The authors concluded that when using dry cutting conditions, the surface roughness is greater the higher the feed rate, but this behavior is non-linear, as when the feed rate is kept constant and cutting speeds increased, roughness rises initially, stabilizes, and then decreases as cutting speed increase. On the other hand, when using wet conditions, roughness tends to decrease continuously with the increase in cutting speed (while maintaining constant feed-rate), leading to the conclusion that higher surface finish is obtained when using low feed-rates, high cutting speeds, and wet cutting conditions [33]. Using the Taguchi methodology, the forces involved regarding end milling cutting processes were investigated taking into account the most important process parameters. It was found that when machining a cast duplex stainless steel under dry cutting conditions, shear forces tended to grow about 21%, 27%, and 46% with depth of cut, cutting speed, and feed rate respectively. In this study, a 1000 rpm spindle speed using 20 mm end mill tool diameter, 63 mm/min of feed rate and 0.4 mm of cut depth were established as optimal cutting conditions for the chosen alloy [34]. Another study sought to determine which combination of cutting conditions promoted the lowest surface roughness and S/N ratio when end milling duplex stainless steel alloys, leading to determine that a 1500 rpm spindle speed, 76.2 mm/min of feed rate and a depth of cut of 1.52 mm was the best condition to achieve the desired results [35], not differing much from the conditions established by the previously mentioned study [34]. Another similar investigation has led to the conclusion that relatively low shear rates, coupled with equally low feed rates, lead to surface quality degradation, mainly due to BUE formation, and optimum machining speeds should be in the range of 220 and 440 m/min, taking into account the use of a relatively low feed rate [36]. Using CD4MCuN duplex stainless steel as the material to be machined, Gouveia et al. [37], with TiAlN coated carbide solid end mill tools concluded that a lower number of flutes in slotting and down milling operations produces a better surface quality than a higher number of flutes, mainly due to the chip extraction process, while a higher number of flutes provides a better surface finish in external squaring and contouring operations. In another study

conducted to investigate the effectiveness of lubrication in the cutting of DSS alloys, it was found that the use of a chlorine-based refrigerant mineral oils and water moisture, promotes higher shear rates and high deterioration of the cutting tool, lead to premature tool deterioration leading to a 65% reduction in tool lifespan [38].

Thus, this work aims to contribute to the extension of the knowledge regarding the mechanisms of wear and vibration level that affect tools during rough milling operations, done so by comparing the behavior of different commercially used coatings and coating techniques, in order to determine the best option to be adopted for these kind of operations as well as which coating behaviors to expect throughout cutting operations.

2. Materials and Methods

In this study, two PALBIT (Albergaria-a-Velha, Portugal) RDHT-type inserts of tungsten carbide (WC) tools with a PVD and CVD coating were used. GX2CrNiMoN26-7-4, a Duplex Stainless-Steel alloy supplied as cast by ARSOPI Company from Vale de Cambra, Portugal was used as workpiece material. Tungsten carbide (WC) was used as substrate material for both the PH7930 and PH5740 inserts, having a round shape geometry with a flank face angle of 13°. The relevant characteristics of the two inserts types are presented in Table 1.

Table 1. Some of the main characteristics of the two insert types.

Insert	Substrate	Coating	Thickness
PH7930	WC	PVD (AlTiN)	7 μm
PH5740	WC	CVD (TiN/TiCN/Al ₂ O ₃)	15 μm

The PH7930 carbide tool inserts were provided with an AlTiN mono-layer coating deposited using PVD. The main deposition parameters used in the coatings' production can be seen in Table 2. The mono-layer AlTiN PVD coating was deposited using TiAl targets in a CemeCom CC800/9ML Unbalanced Magnetron Sputtering system (CemeCon, Würselen, Germany). The CVD multi-layer coating was synthesized using a SuCoTec SCT600 TH (Sucotec, Langenthal, Switzerland) industrial-scale low-pressure CVD.

Table 2. Main data about the coatings' deposition processes. PVD: physical vapor deposition; CVD: chemical vapor deposition.

Insert	Coating	Deposition Time	Thickness	Deposition Temperature	Used Gases	Pressure
PH7930	PVD (AlTiN)	110 min	7 μm	450 °C	Ar ⁺ + Kr	500 mPa
PH5740	CVD (TiN/TiCN/Al ₂ O ₃)	260 min	15 μm	900 °C	TiCl ₄ + CH ₄ +N ₂ + H ₂ + Al(C ₅ H ₇ O ₂) ₃	100 mbar

Figure 1a illustrates the WC substrate; and Figure 1b the AlTiN coating microstructure, both with a magnification of 1500 \times . The micro-hardness of these inserts after coated is 3515 HV₃₀ \pm 62 HV₃₀. The micro-hardness was assessed through ten indentations carried out in a Micro-hardness Fisherscope H100 micro-hardness tester (Fischer Technology, Windsor, CT, USA.) using a normal load of 50 mN and dwell time of 30 seconds, avoiding by this way creep phenomenon. The selected load took into account that the depth of penetration cannot exceed 10% of the coating thickness, as referred in [39]. Indeed, the maximum depth registered does not surpassed 8% of the coatings' thickness. "Load-Depth" curves were interpreted, and computed the revised (E') Young's modulus as 482.72 \pm 23.84 GPa. These values are in line with the values obtained in other works [39].

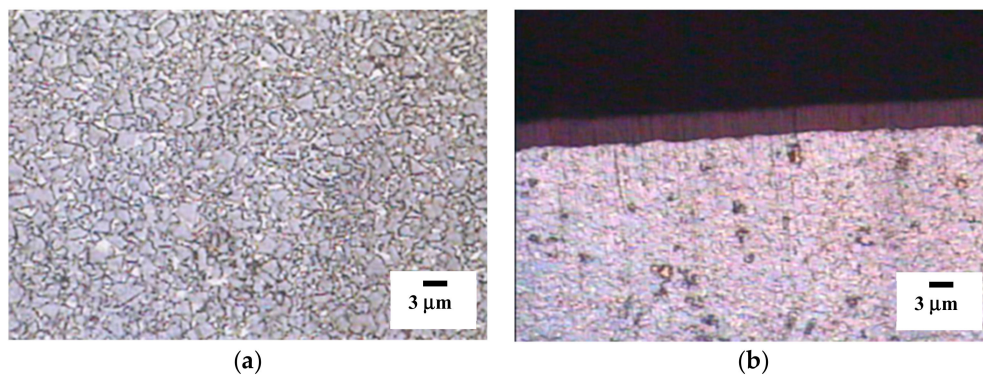


Figure 1. (a) Top view of the WC PH7930 micro-grain sintered microstructure (1500×); (b) AlTiN coating + substrate microstructure in cross-section view (1500×) (Courtesy of Palbit).

Table 3 presents the chemical composition, as well as the physical and mechanical properties of the PH7930 substrate, provided by the vendor PALBIT.

Table 3. Chemical composition, physical and mechanical properties of the PH7930 substrate.

Chemical Composition (wt%)	
% Co	10.00 ± 0.20
% γ (TaC + NbC + TiC) + other	(0.5–1.5)
% WC	Balance
Grain size of WC used in the mixture ≈ 3.0 μm	
Physical and mechanical properties in sintered state	
Hardness	1385 ± 40 (HV10)
Transverse Rupture Strength (Bend)	3100 N/mm ²

Then, the PH5740 carbide tool inserts were coated by CVD technique using a TiN/TiCN/Al₂O₃ multi-layered system. Figure 2a depicts the WC substrate microstructure and Figure 2b the TiN/TiCN/Al₂O₃ coating microstructure, both with a magnification of 1500×. The micro-hardness of these inserts after coating is 3315 HV₃₀ ± 55 HV₃₀. The procedure followed for micro-hardness measurement was the same as above. No values were found in the literature that could correspond to the same sequence of coatings, performed under the CVD technique and with the same thickness. “Load-Depth” curves were interpreted and computed the revised (E′) Young’s modulus as 458.91 ± 25.82 GPa. However, the values obtained for the coating used in this work are higher than those reported by other similar coatings [40,41].

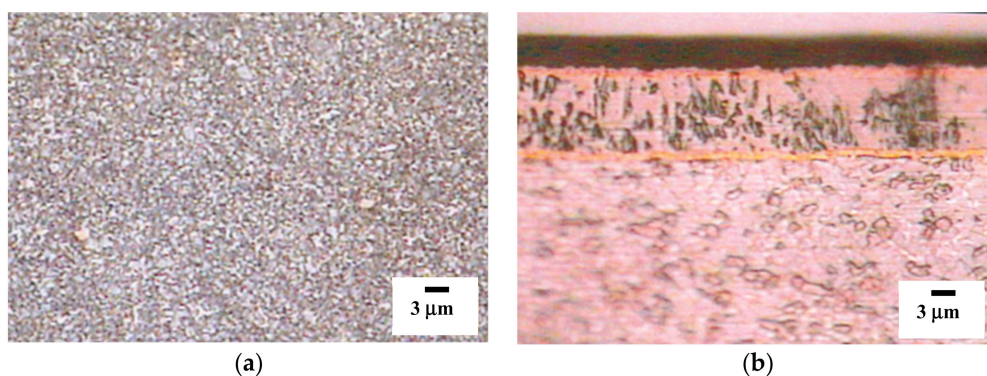


Figure 2. (a) Top view of the WC PH5740 micro-grain sintered microstructure (1500×); (b) Al₂O₃ coating + substrate microstructure in cross-section view (1500×) (Courtesy of Palbit).

Table 4 presents the chemical composition, as well as physical and mechanical properties of the PH5740 substrates, provided by the vendor PALBIT.

Table 4. Chemical composition and physical and mechanical properties (PALBIT).

Chemical Composition (wt%):	
% Co	11.50 ± 0.20
% γ (TaC + NbC + TiC) + other	(1.0–2.0)
% WC	Balance
Grain size of WC used in the mixture \approx 0.8 μ m	
Physical and mechanical properties in sintered state	
Hardness	1480 ± 40 (HV10)
Transverse Rupture Strength (Bend)	3500 N/mm ²

As referred previously, the material used as workpiece in these tests was a Duplex Stainless Steel (DSS), ASTM A890, World No. 1.4501, DIN 17445 GX2CrNiMoN26-7-4 grade (ARSOPI, Vale de Cambra, Portugal). The chemical composition (wt%) given by the supplier for this batch of DSS is presented in Table 5.

Table 5. Chemical composition (wt%) of DSS DIN 17445 grade GX2CrNiMoN26-7-4.

C	Si	Mn	P	S	Cr	Ni	Mo	Cu	Nb	V	W	N	Fe
0.03	1.00	1.00	0.035	0.015	26.00	8.00	4.00	1.00	0.01	0.02	1.00	0.30	balance

According to the supplier, the DSS used presents a 290 HB hardness, a yield strength (0.2%) of 500 MPa and an ultimate tensile strength of 710 MPa.

Milling tests were performed in a HAAS CNC machining center (HAAS Automation, Oxnard, CA, U.S.A.), model VF-2, with 22.4 kW maximum power, 10,000 rpm maximum spindle speed and 122 Nm@2000 rpm maximum torque. Tool wear was analyzed and measured using a scanning electron microscope (SEM) FEI Quanta 400 FEG (Field Electron and Ion Company, Hillsboro, OR, USA). The roughness of the DSS machined surface was assessed using a MAHR M2 profilometer (Mahr, Göttingen, Germany), provided with a diamond stylus tip with a 2 μ m radius (ISO 4288:1996) [42]. After each test the evaluation of the surface roughness was analyzed by measuring R_a , R_z , and R_{max} (the three parameters generally used to characterize the quality of machining surfaces). Two different roughness measurements were taken, one in a radial orientation and the other in a tangential orientation, using a cutoff value of 0.8 mm. Tool degradation progress was observed via vibration levels analysis. The vibration levels produced during all tests were evaluated with two PCB accelerometers (PCB Piezotronics, Depew, NY, USA), model 352A24, coupled onto the machine spindle. The data collected was processed using LabVIEW® 2017 software.

In all milling tests, a spiral pathway was used, as represented in Figure 3a. The cutting tools used are of RDHT type, whose geometry is shown in Figure 3b. The cutting inserts have a circular shape, allowing to be rotated up to three positions regarding the cutting edge (120° each rotation). The tool holder used is represented in Figure 3b, presenting 16 mm diameter with two insert support housings. This type of insert is usually used for milling operations. For the machining tests, RDHT type inserts of different classes, PH7930 and PH5740 grades were used.

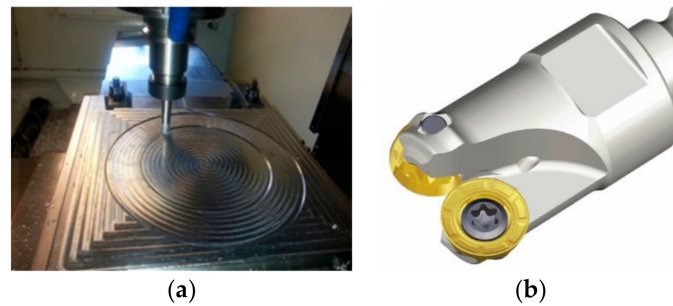


Figure 3. (a) Machining strategy used in all tests; (b) tool holder (www.taegutec.com).

The parameters and conditions of the tests, imposed exclusively by the manufacturer of the inserts, were kept unchanged in all performed tests and are as follows: cutting speed $V_c = 76.2$ m/min, rotational speed $n = 1516$ rpm, feed $f_z = 0.15$ mm/rev, number of teeth $Z = 2$, and tool holder diameter $D_c = 16$ mm with the reference 15E2R028M08-SRD07, using inserts with 7 mm diameter. The cutting width used was 75% of the cutting tool diameter. These parameters correspond clearly to a rough milling operation, as intended in this work. Throughout all tests, the depth-of-cut ($a_p = 1$ mm) remained constant. The main tools' characteristics and cutting length are shown in Table 6. In these tests, dry cutting conditions based on the results obtained by [38] were used in an effort to promote the most severe milling test conditions.

Table 6. Cutting insert reference, coating and cutting length for each test.

Test	Cutting Insert	Coating	Thickness	Times	Cutting Length
1	PH7930	PVD (AlTiN)	7 μ m	3	3.94 m
2					
3					7.87 m
4					
5	PH5740	CVD (TiN/TiCN/Al ₂ O ₃)	15 μ m	3	3.94 m
6					
7					7.87 m
8					

AlTiN coatings were produced via PVD using an industrial CemeCon CC800/9ML PVD Magnetron Sputtering system; TiN/TiCN/Al₂O₃ multilayer coatings were produced using an industrial-scale low-pressure CVD equipment SuCoTec SCT600 TH (Sucotec, Langenthal, Switzerland), in which the titanium coatings are formed by reacting titanium tetrachloride (TiCl₄) with mixtures of nitrogen (N₂) and methane (CH₄), in varying portions to tailor the coating stoichiometry depending on the final application. Aluminum oxide (Al₂O₃) is a two-step synthesis process formed by the reaction of aluminum trichloride (AlCl₃) with carbon dioxide (CO₂) to form Al₂O₃. AlCl₃ is formed in an external halide gas generator by passing hydrogen chloride (HCl) gas over pellets containing aluminum. The synthesis' parameters were considered confidential by the tools' manufacturer.

Topography of the workpiece's machined surfaces was monitored using a MAHR M2 profilometer (Mahr, Göttingen, Germany). Morphology of the PVD TiAlN coated carbide tool's worn surfaces (flank and rake faces) as well as chip surfaces were characterized using a scanning electron microscope (SEM). Energy dispersive x-ray analysis (EDX), backscattered electron imaging of the surface and the generated vibrations along the milling tests were also analyzed. The aim of the tests was the comparison of the behavior of inserts provided with the two types of coatings previously mentioned.

In this work, eight machining tests were carried out under dry conditions, as can be observed in Table 6. Two cutting lengths were used: a short one ($S = 3.94$ m) and a long one ($L = 7.87$ m). For each cutting length, two experiments have been done, leading to S1/S2 or L1/L2 trials references.

Because of the circular shape of the cutting inserts, each one was rotated up to three positions, which meant a total of twenty-four trials. During the tests, the vibrations level in the two orthogonal directions was collected. The surface roughness was measured after each test. At the end of the tests, all cutting tools were analyzed by SEM and, when necessary by EDS (Energy-Dispersive X-ray Spectroscopy), being the tool flank face wear (VB) and the tool rake face wear (KB) markings assessed by SEM, both for the PVD PH7930 and CVD PH5740 coated carbide inserts. The results shown in this work correspond to the inserts with the most significant wear marks. The fixation of the inserts in the chamber of the SEM equipment always followed the same protocol, in order to guarantee the effectiveness and efficiency of the wear marks measuring process.

3. Results

After each test, the quality of the resulting surface was conveniently evaluated by profilometry, analyzing the previously mentioned parameters: R_a , R_z , and R_{max} , in order to correlate the state of the machined surface with the wear phenomena identified in the corresponding tools.

The analysis of vibrations was also accessed and dissected through the graphs resulting from the signals sent by the accelerometers, which were transformed into values and placed in graphic form, allowing to verify the level of vibration at each moment of the test. Special care was taken in fixing the tool holder, tightening the inserts and attaching the workpiece to the machine's work table, in order to eliminate as much as possible, the appearance of external phenomena that could prevent an adequate reading of the results.

In parallel, the performance of the cutting tools during the milling operation was observed with videos images taken by a high-speed camera (brand Photron, model Fastcam SA4, San Diego, CA, U.S.A.), during the experimental tests (Figure 4). The flank face angle and the chip breaker selected for these inserts did not show good results, probably due to the high mechanical strength of the workpiece material. Occasionally, the chip also remained adhered to the tool for too long, which possibly caused premature tool break, increasing the probability of fracture of the cutting edge and consequently a rougher surface finish of the part.



Figure 4. Image obtained from the video by a high-speed camera, during the experimental tests.

Taking into account the number of tests performed, as described in Table 6, the results shown below are organized by sub-sections and tables, systematizing the information to be highlighted.

3.1. PH7930-S1 and -S2 Tests (PVD AlTi- Coated Tools)

The milling tests with PVD PH7930 and CVD PH5740 coated inserts were made under the conditions and parameters previously described. Table 7 shows the surface roughness for the PH7930 end mill machining tests with a “short” cutting length of 3.94 m (S).

Table 7. Surface roughness for the workpiece surface generated by PH7930 PVD AlTiN coated insert with a cutting length of 3.94 m (S).

Test	<i>Ra</i> (μm)		<i>Rz</i> (μm)		<i>Rmax</i> (μm)	
	PH7930-S1	PH7930-S2	PH7930-S1	PH7930-S2	PH7930-S1	PH7930-S2
1	0.857	0.493	4.300	3.300	5.810	3.950
2	0.862	0.579	6.320	3.500	6.600	5.060
3	0.802	0.593	4.270	4.310	4.680	6.060
Average	0.840	0.555	4.963	3.703	5.697	5.023
Std Dev. ±	0.027	0.044	0.959	0.437	0.788	0.862

The analysis of Table 7 shows slightly higher values of *Ra* and *Rz* for the PH7930-S1 tool insert. These results are in agreement with the images obtained via SEM, depicted in Figure 5 representing the failure seen on the PH7930-S1 tools' cutting-edge. In this case, corresponding to a short cutting distance, it is clearly a homogeneous and slight failure of the substrate (carbide grade), and not a failure of the coating, being evident the marginally broken edge of the insert (Figure 5, left side). This analysis reveals that for the short cutting distance inserts shows small signs of failure with fractures at the cutting edge, with a VB of 222.5 μm and KB of 147.5 μm. The other insert had a less homogeneous flank wear along the cutting edge, with a VB of 70.03 μm and KB of 262.5 μm in the critical zone, but with no clear signs of coating failure. On the left side of the worn area and in the critical zone, there are clear signs of abrasion wear. This case corresponds to the same machining distance and, despite the lower flank wear, the degradation of the insert in the top side of the tool is higher, leading to an increased rake face wear. The clear abrasion effect mark is a result of the chip flow in that area. The wear phenomenon did not depend on the coating performance, because there is a clear rupture of the substrate material (carbide). The remaining coated surface of the tool keeps a non-degraded appearance, showing that the coating seems to not feel the abrasion effect of the chip flowing over its surface. The larger worn area in the second insert under the same test conditions can upsurge from some heterogeneity of the workpiece material, which leads subsequently to a higher degradation of the cutting edge.

The evolution of the vibration amplitude presented in Figure 6a, related to one of the PH7930-S1 tests does not allow to identify any occurrence of failure in the cutting inserts. This is in agreement with the images obtained by SEM. On the contrary, Figure 6b shows the time course of the RMS level for the vibration regarding the PH7930-S2 test which shows the appearance of a vibration peak of 0.2 mm/s, close to 200 s. Although this is not a very significant value, it represents the moment where the cutting inserts came in contact with some heterogeneity of the workpiece material, or it could simply have been the first sign of tool failure, which eventually evolved during the course of the test. The increase of vibration levels after 200 seconds shows the premature wear of the tool. In the YY' axis it should be seen that the scale is completely different, being clear that the phenomenon induced in the insert relative to the test PH7930-S2 test has a magnitude substantially higher than the vibration level sensed in the first short duration test (PH7930-S1). This may have as origin the following causes: small heterogeneity found by the insert in the Duplex Stainless-Steel raw material, or sudden failure of the cutting edge. As can be seen in Figure 5 (d), there is a much more pronounced failure in this insert than in the insert being analyzed together (PH7930-S1), whereby the second reason given above is the more likely, although this cutting edge rupture can also be caused by a heterogeneity of the machined material.

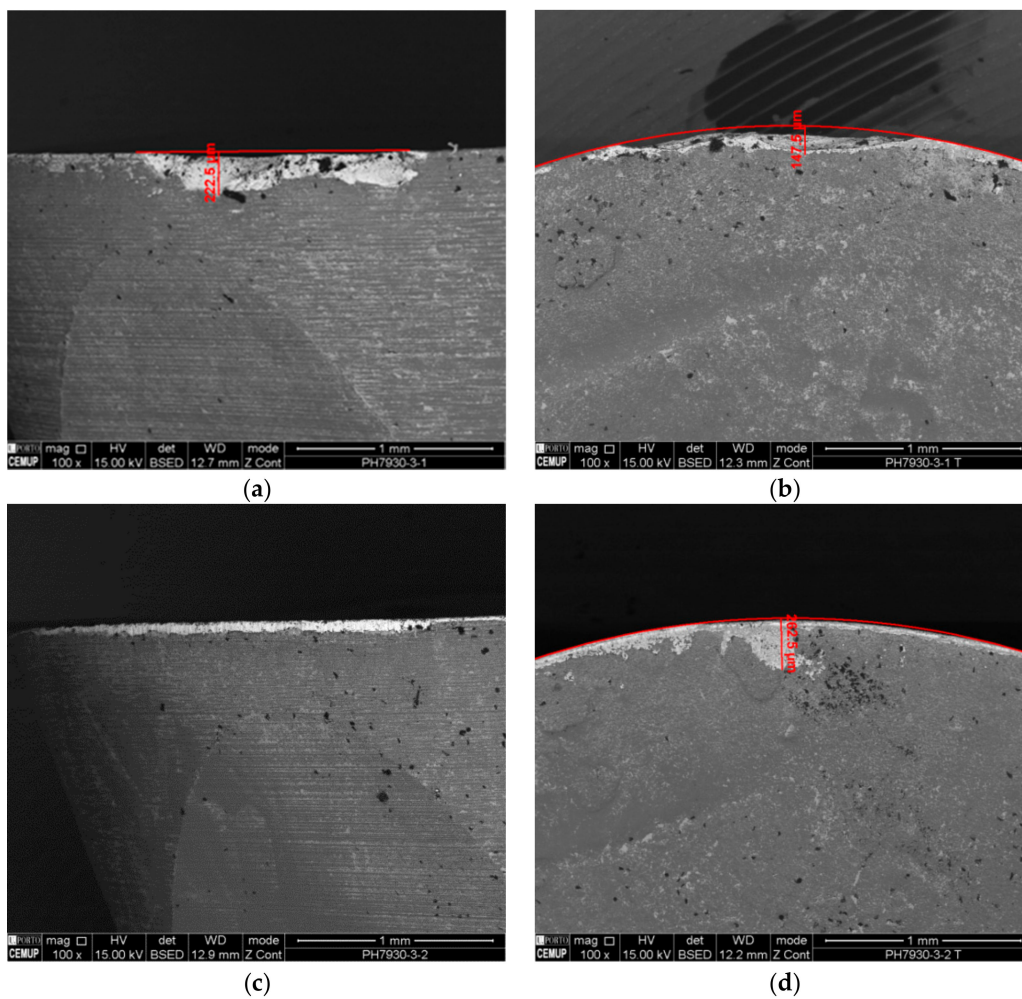


Figure 5. (a) and (c) flank wear (VB) of PVD PH7930-S1 and PH7930-S2 cutting inserts, respectively; (b) and (d) rake face/land wear (KB) of PVD PH7930-S1 and PH7930-S2 cutting inserts, respectively.

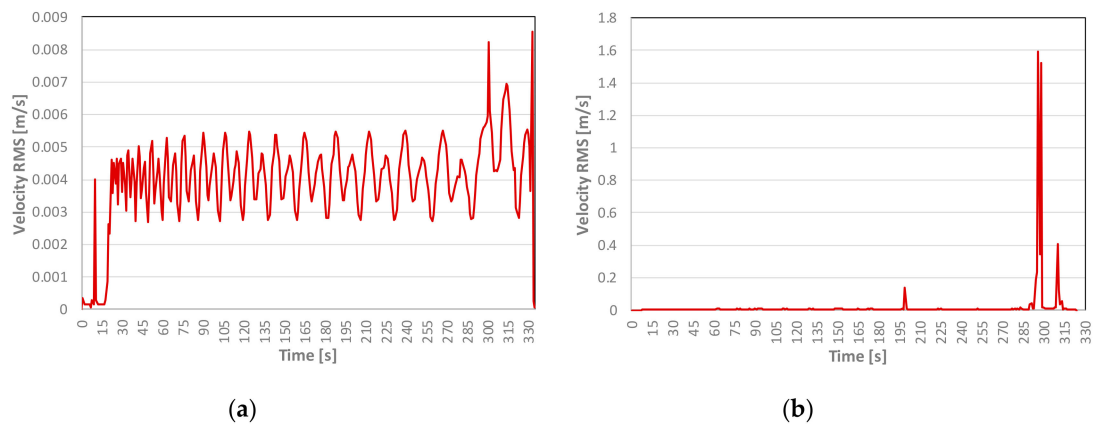


Figure 6. Vibrations amplitude on PVD coated inserts for the group of tests of (a) PH7930-S1 and (b) PH7930-S2 cutting inserts.

3.2. PH7930-L1 and L2 Tests (PVD AlTiN Coated Tools)

Table 8 shows the surface roughness assessment for the surface produced by the PH7930 PVD coated insert, corresponding to the “long” cutting length of 7.87 m (L).

Table 8. Surface roughness for the workpiece surface generated by PH7930 PVD AlTiN coated insert with a cutting length of 7.87 m (L).

Test	<i>Ra</i> (μm)		<i>Rz</i> (μm)		<i>Rmax</i> (μm)	
	PH7930-L1	PH7930-L2	PH7930-L1	PH7930-L2	PH7930-L1	PH7930-L2
1	0.857	0.622	5.010	5.940	6.410	5.190
2	0.788	0.730	5.460	4.400	7.220	4.740
3	0.786	0.779	4.620	5.370	5.430	6.660
Average	0.810	0.710	5.030	5.237	6.353	5.530
Std Dev. ±	0.033	0.066	0.343	0.636	0.732	0.820

The images of the PH7930-L1 and PH7930-L2 cutting tools, obtained by SEM can be seen in Figure 7. One of the cutting tools shows a flank face wear (VB) of 128.8 μm (Figure 7a) and a rake face wear (KB) of 335.1 μm (Figure 7b) with a loss of coating. The other insert exhibits a flank wear of 136.5 μm (Figure 7c), a rake face wear of 302.7 μm (Figure 7d) and signs of fracture at the cutting edge. Indeed, despite the coating and substrate being the same, the behavior of the tools is different. Under long cutting distance conditions flank wear is evident as well as small fractures, as happened in the short distance tests although with less severity. On the other hand, the extension of the damage is larger in both cases shown in Figure 7 and, in this case, spalling phenomenon has occurred, with coating detachment or wear however, the substrate carbide material seems to support the efforts promoted by the machining process. As the damage of the substrate is not significant, it is believable that the coating had detached from the substrate recently, regarding the breaking phenomenon shown in Figure 5. There are other small and punctual coating detachments along the tool's top surface, showing that the DSS material flow generates enough abrasion to damage the coating. No BUE or adhesive wear phenomena close to the cutting edge seem to affect the tool, as no visible adherent material can be seen close to the edge. Regarding these tests, wear behavior was very similar, as well as the VB and KB values.

A confirmation of the coating composition was performed by EDS X-Ray micro-analysis (Figure 8), verifying its existence in the darker areas of Figure 7 (Z1—Zone 1—Flank face). It was possible to identify the coating composition, presented in Figure 8. Its composition is based on Titanium and Aluminum, corresponding to the AlTiN layer deposited by PVD technique. The clearer areas show the substrate color, thus, the absence of coating, corresponding to worn areas.

Its composition reveals a clear presence of the coating, but with slight signs of partial loss. This phenomenon occurs due to the natural wear caused by friction of the insert in the workpiece. Small white dots are also observed along the surface, which are caused by the impact of the removed chips on the top surface of the tool, as previously referred.

The analysis of the RMS vibration level related to the PH7930-L1 test, shown in Figure 9a, allows stating that vibration level remain practically constant throughout the test. At the instant close to 320 seconds, a disturbance in vibration amplitude was observed, which indicates the change from the first to the second machining cycle (short to long cutting distance) however, the amplitude is insignificant. Figure 9b shows some peaks in the vibration level, being the first detected after 298 s, reflecting the progressive degradation of the cutting tool. In this second case, the amplitude of the signal registered is significant. As in the case of PH7930-S2 insert, the origin of the higher amplitude of this signal (Figure 9b) can be attributed to raw material small heterogeneities or sudden failure of the cutting edge, as can be seen in Figure 7d. However, in this case, the rupture of the tool edge seems occur in the final phase of the test, where the more intense peaks start to be more frequent. Thus, the first strong peaks can be attributed to raw material heterogeneities, whereas the last more intense peaks reflects a progressive degradation of the cutting edge.

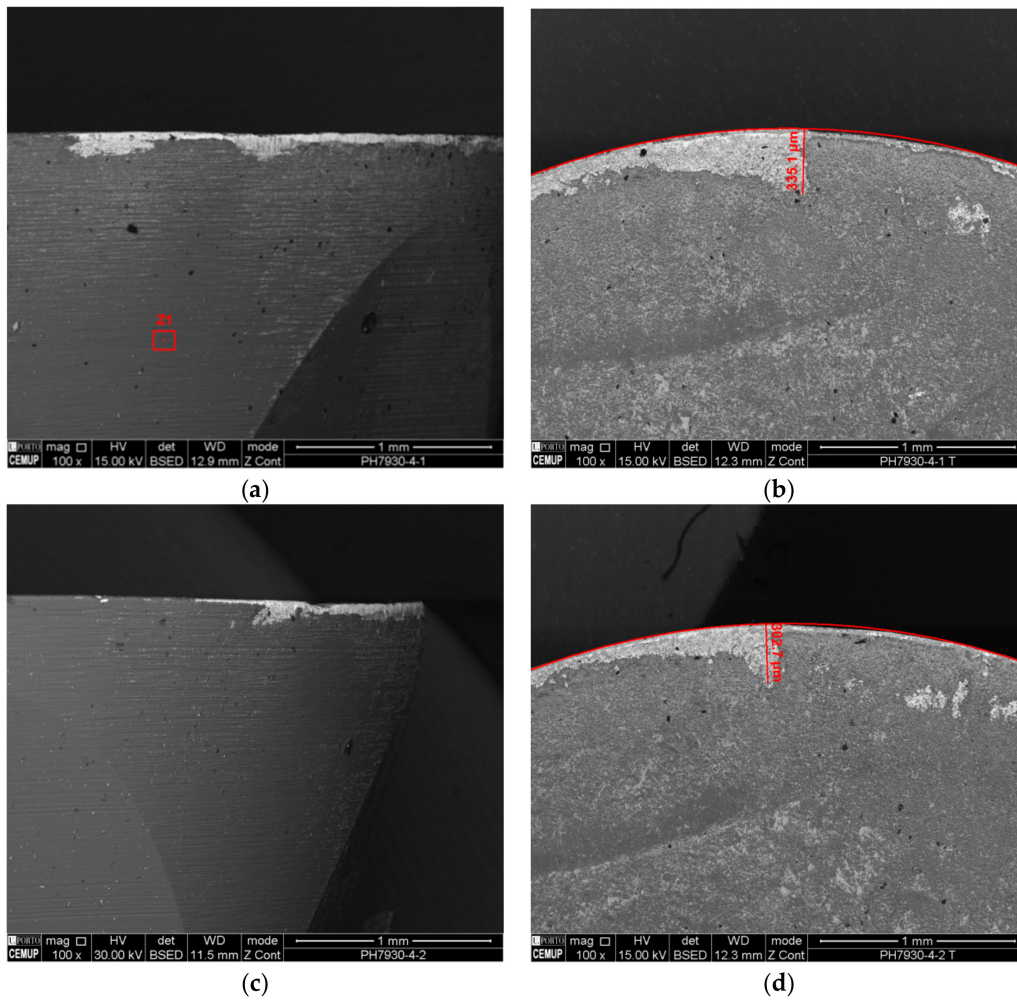


Figure 7. (a) and (c) Flank wear (VB) of PVD PH7930-L1 and PH7930-L2 cutting inserts, respectively; (b) and (d) rake face/land wear (KB) of PVD PH7930-L1 and PH7930-L2 cutting inserts, respectively.

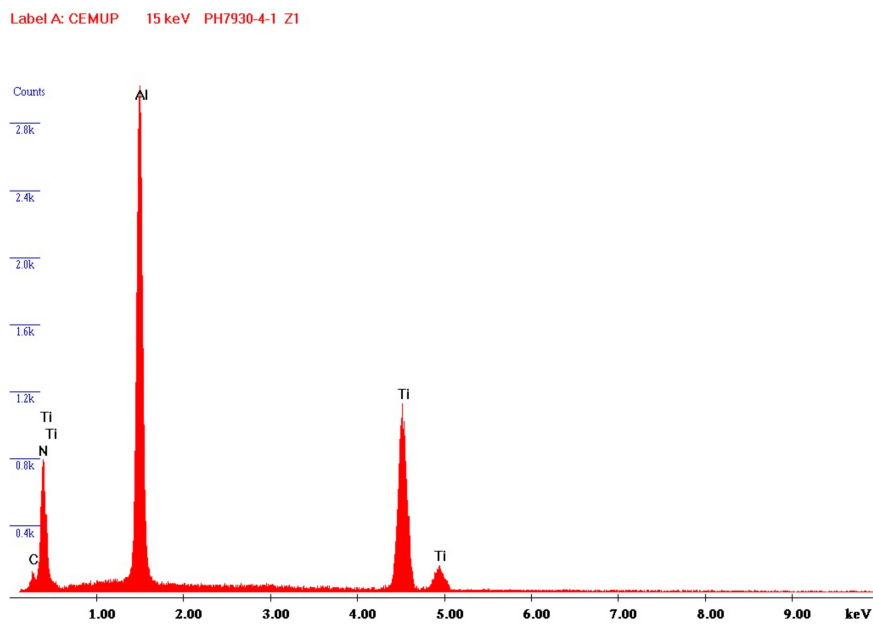


Figure 8. EDS spectrum of the Zone 1 pointed out in the SEM image of Figure 7a.

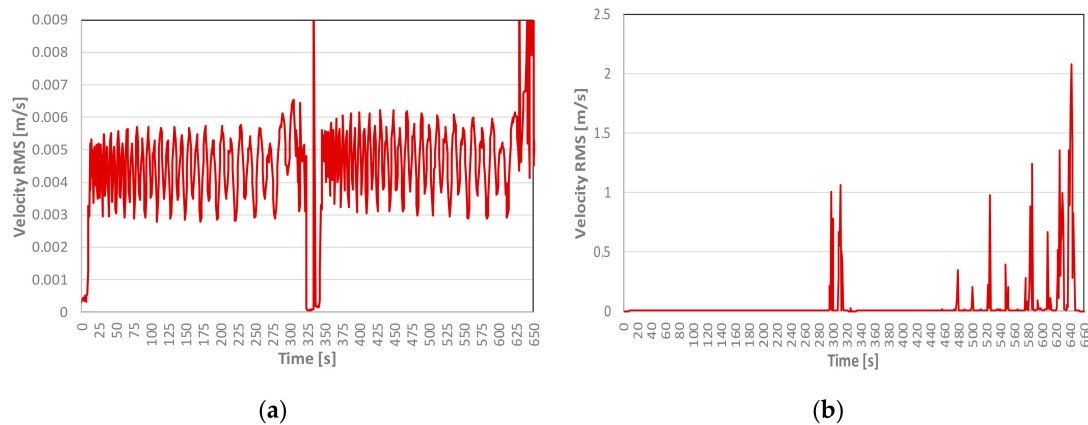


Figure 9. Vibrations amplitude on PVD AlTiN coated inserts for the group of tests corresponding to (a) PH7930-L1 and (b) PH7930-L2 cutting tests.

3.3. PH5740-S1 and S2 Tests (CVD TiN/TiCN/Al₂O₃ Coated Tools)

Table 9 shows the surface roughness assessment for the surface produced by the PH5740 end mill with a “short” cutting length of 3.94 m (S).

Table 9. Surface roughness for PH5740 CVD TiN/TiCN/Al₂O₃ coated inserts with a cutting length of 3,94 m (S).

Test	Ra (μm)		Rz (μm)		Rmax (μm)	
	PH5740-S1	PH5740-S2	PH5740-S1	PH5740-S2	PH5740-S1	PH5740-S2
1	0.599	1.033	4.100	5.070	7.870	5.940
2	0.783	0.977	5.900	5.260	9.570	8.090
3	0.626	0.995	4.300	5.200	8.370	6.110
Average	0.669	1.002	4.767	5.177	8.603	6.713
Std Dev. ±	0.081	0.023	0.806	0.079	0.713	0.976

The images of CVD coated cutting tools obtained by SEM, are presented in Figure 10. In these images it is possible to identify a greater flank wear (VB), compared with PVD cutting tools. One of the cutting inserts presents a VB of 512.5 μm and KB of 218.2 μm and the other having a maximum VB of 447.5 μm and KB of 287.5 μm. In comparison with the images from Figure 5, it is clear that the damage produced in the CVD coated tools is significantly higher than the damage endured by the PVD AlTiN coated tools. There is a clear degradation of the flank face, with extended flank wear. No clear crater/land wear is observed but the coating disappeared in the more loaded areas and, after that, the substrate seems to not be strong enough to keep its integrity. Thus, in the areas where the coating is gone damage of the substrate is clear, as referred in [13]. In Figure 10a there is an exception, because there is a small area where the films does not exist, but the substrate is not clearly damaged. Thus, it remains clear that this coating seems to present a britler behavior and the carbide grade presents some difficulties to remain integral after coating detachment or wear. There are no clear evidences of neither abrasion nor adhesive wear in the areas that remain able to be analyzed. It is possible that BUE formation could have occurred on the cutting edge and afterwards the loads in that area promoted cutting edge breakage.

The vibration levels assessed in both PH5740-S1 and PH5740-S2 tests are shown in Figure 11. In these tests, no clear incidents in vibration levels were identified, which could be associated with premature failure of the tools. This behavior shows that wear was progressive, throwing aside any speculation regarding the formation of a possible BUE, which was referred in [28,29]. Indeed, the wear and tear must have begun to occur on the coating, which deteriorated progressively, resulting in degradation of the substrate. This entire process must have been sufficiently continuous and homogenous, so as not to cause any disturbance in the reading of vibration levels. With this type of

wear, and although the tool is quite deteriorated, the effect on the quality of the machined surface is not as significant as a localized fracture of the substrate, allowing relatively good values to be obtained for the roughness of the machined surface. In spite of the vibration level values being low and remaining constant during the tests, in the PH5740-S2 test at 73 s, a small variation of the vibration was identified, which can identify the moment of the first tool failure that justifies the average roughness values higher than the PH5740-S1 test.

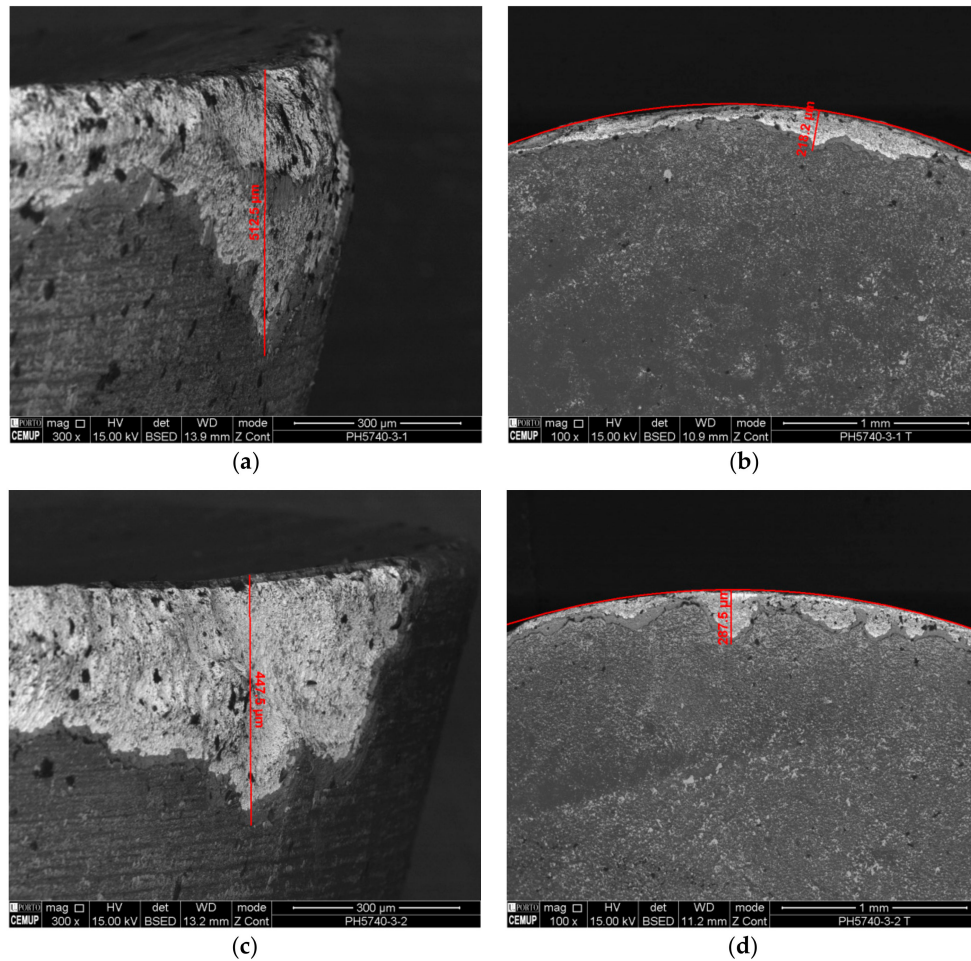


Figure 10. (a,c) flank wear (VB) of CVD TiN/TiCN/Al₂O₃ PH5740-S1 and PH5740-S2 cutting inserts, respectively; (b,d) crater wear (KB) of CVD TiN/TiCN/Al₂O₃ PH5740-S1 and PH5740-S2 cutting inserts, respectively.

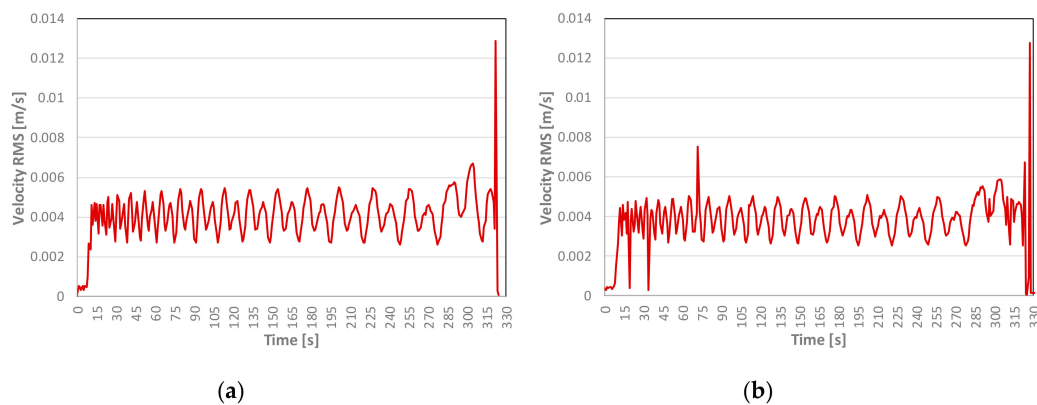


Figure 11. Vibrations amplitude corresponding to CVD TiN/TiCN/Al₂O₃ coated inserts for two of the machining tests (a) PH5740-S1 and (b) PH5740-S2 cutting inserts.

3.4. PH5740-L1 and L2 Tests (CVD TiN/TiCN/Al₂O₃ Coated Tools)

Table 10 shows the surface roughness assessment for the surface produced by the PH5740 end mill with a “long” cutting length of 7.87 m (L). These tests show similar values of Ra, Rz and Rmax comparing with the previous tests corresponding to the short cutting length under the same cutting parameters.

Table 10. Surface roughness of PH5740 CVD TiN/TiCN/Al₂O₃ coated inserts with a cutting length of 7,87 m (L).

Measurements PH5740	Ra (μm)		Rz (μm)		Rmax (μm)	
	PH5740-L1	PH5740-L2	PH5740-L1	PH5740-L2	PH5740-L1	PH5740-L2
1	0.804	0.814	4.680	5.060	7.410	8.070
2	0.626	1.029	3.290	4.790	4.840	6.610
3	0.659	1.488	4.770	6.980	5.480	7.860
Average	0.696	1.110	4.247	5.610	5.910	7.513
Std Dev. ±	0.077	0.281	0.677	0.975	1.092	0.644

Figure 12 shows the images obtained by SEM at the end of the CVD PH5740 tests. The analysis of these images shows that the tests with this type of cutting inserts present greater wear than in the short length tests. One of the inserts presents VB of 875.6 μm and KB of 278.1 μm, and the other insert presents several fractures and craters at the cutting edge, with VB of 848.3 μm and KB of 224.2 μm. The phenomena induced in these cases are very similar to the ones observed under a short cutting length, but the wear effect is more pronounced, with small punctual breakages of the cutting edge, though not enough to affect significantly the surface quality of the machined workpiece, as the wear is almost uniform along the cutting edge. Thus, the roughness values are not significantly changed from the first case to this one.

Figure 13a,b shows the vibration level during the PH5740-L1 and PH5740-L2 tests, respectively. From the analysis of the vibration level it is not possible to identify in both tests perturbations that can be associated with the abrupt failure of the cutting tool, although they present values in different maximum amplitude. The recorded vibration level of the PH5740-L2 tests was higher, justifying this way the roughness values obtained.

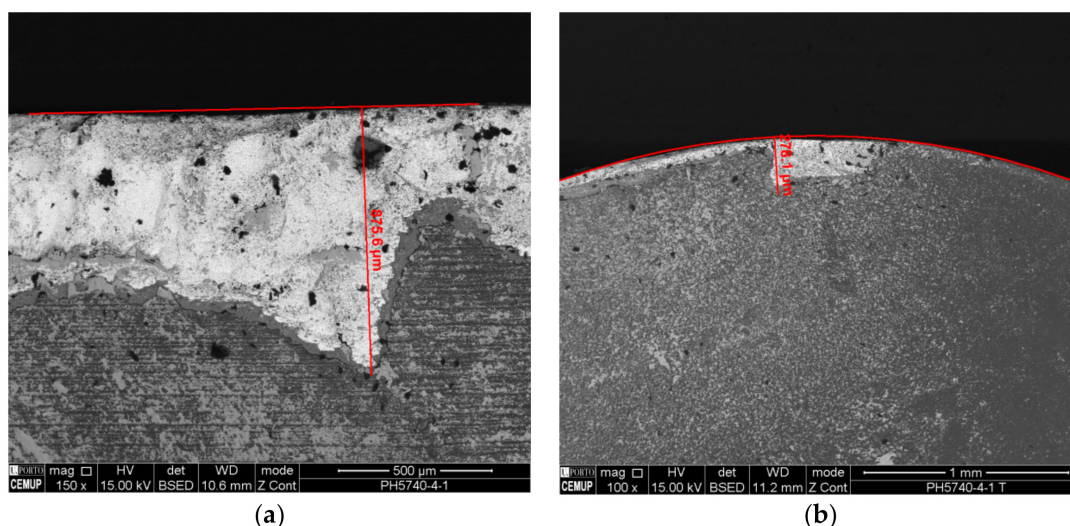


Figure 12. Cont.

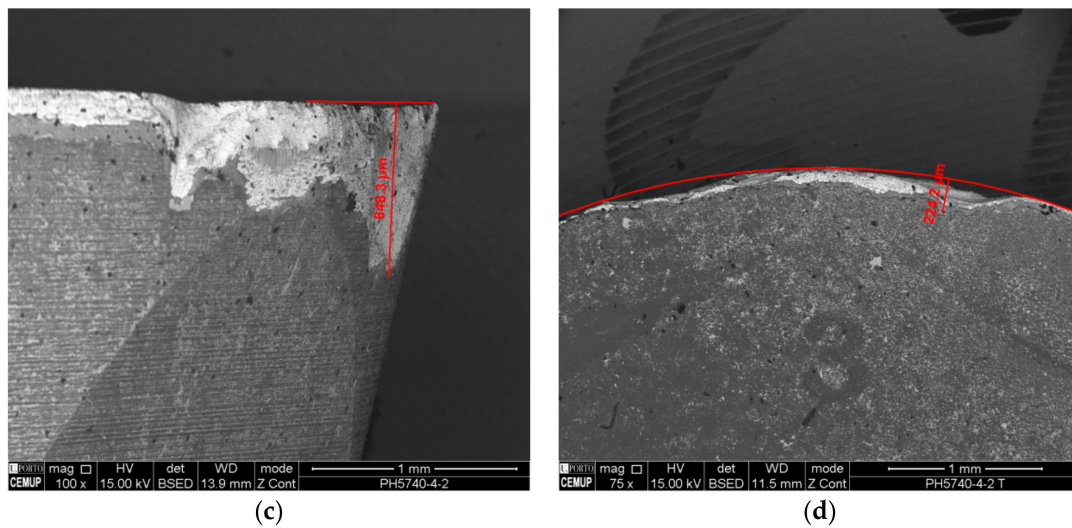


Figure 12. (a) and (c) flank wear (VB) of CVD PH5740-L1 and PH5740-L2 cutting inserts, respectively; (b) and (d) crater wear (KB) of CVD PH5740-L1 and PH5740-L2 cutting inserts, respectively.

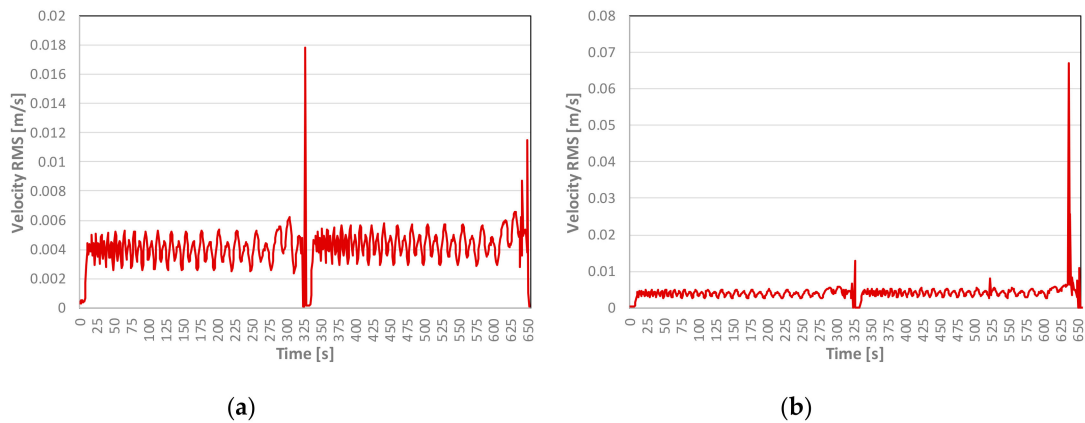


Figure 13. Vibrations amplitude on CVD coated inserts for (a) PH5740-L1 and (b) PH5740-L2 cutting inserts tests.

3.5. Overall Analysis

3.5.1. Roughness

In order to evaluate tool wear, the quality of the surfaces of the DSS alloys was assessed by measuring the roughness of the machined surfaces at the end of each test. Under these conditions, the values of the parameters Ra , Rz , and $Rmax$ were evaluated and summarized in Table 11.

Table 11. Average surface roughness for all tests with both PVD and CVD coated inserts.

PVD Inserts				CVD Inserts			
Test	Ra (μm)	Rz (μm)	$Rmax$ (μm)	Test	Ra (μm)	Rz (μm)	$Rmax$ (μm)
PH7930-S1	0.840	4.963	5.697	PH5740-S1	0.669	4.767	8.603
PH7930-S2	0.555	3.703	5.023	PH5740-S2	1.002	5.177	6.713
PH7930-L1	0.810	5.030	6.353	PH7930-L1	0.696	4.247	5.910
PH7930-L2	0.710	5.237	5.530	PH7930-L2	1.110	5.610	7.513

In this analysis overview, variations of roughness were identified, according to the tool used and the duration of the tests. Based on Table 11 it was verified that PH7930 tools produced a better surface finish than PH5740 tools

3.5.2. Wear

After all the tests, similar wear on the cutting tools was found. Failures like fractures, flaking, or delamination of the coating occurred on the surface and cutting edge and flank wear. All these failures provoked the increase of workpiece surface roughness. It was also verified that the inserts that showed the greatest wear, presented a better surface finish. It means that PVD AlTiN coating showed to be more suitable for end milling operation of this kind of DSS alloy than the CVD TiN/TiCN/Al₂O₃.

3.5.3. Vibrations

The vibration analysis during the tests showed that PH7930 tools have higher vibration levels, and also presented a greater number of unexpected failures. The severe increase in the level of vibration during the tests allowed to identify the moment of tool failure or when the wear began to be accentuated. Regarding the level of vibration produced by PH5740 tools, it always remained lower and more stable, which resulted in a smaller number of failures, as can be seen in Table 12. However, the wear is more accentuated in PH5740 CVD coated tools, although being more homogeneous than in the PH7930 PVD coated tools. The moments of the first failure occurrence in the tool, identified by the abrupt increase in vibration level, are indicated in Table 12.

Table 12. Time of failure occurrence.

Insert	Total Test Time (s)	Time of Occurrence (s)
PH7930-S1	315	-
PH7930-S2	315	289
PH7930-L1	630	487
PH7930-L2	630	-
PH5740-S1	315	-
PH5740-S2	315	-
PH5740-L1	630	-
PH5740-L2	630	-

3.5.4. Chip Analysis

Chips generated by the two different coated cutting tools were studied. Figure 14a shows the type of chip obtained during the milling tests. Chips were collected after the machining tests and analyzed by SEM. Chips are characterized to be short and fragmented, which present irregularities at the ends, as shown in Figure 14b. These irregularities are a sign of the difficulty in extracting the chip and friction involved. They also have a crushing zone, with successive grooves, due to the high cutting effort generated by the flank face angle. As can be seen in Figure 14a, the chips exhibit high plastic deformation.

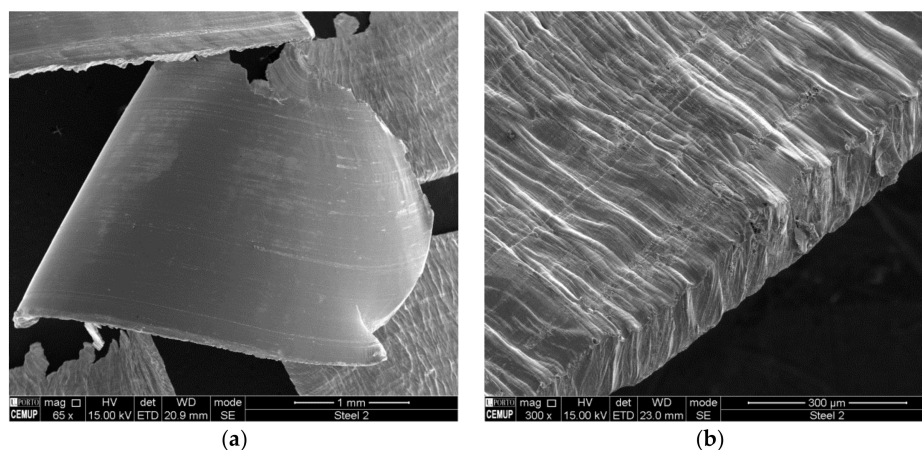


Figure 14. Chip obtained during the milling trials ((a) and b)).

As represented in Figure 15a, small fragments retained in the chips have also been detected, and chemically analyzed by EDS. According to Figure 15b, it was identified that these fragments are parts of the inserts coating, indicating coating removal or detachment. This phenomenon has already been reported in similar works [43].

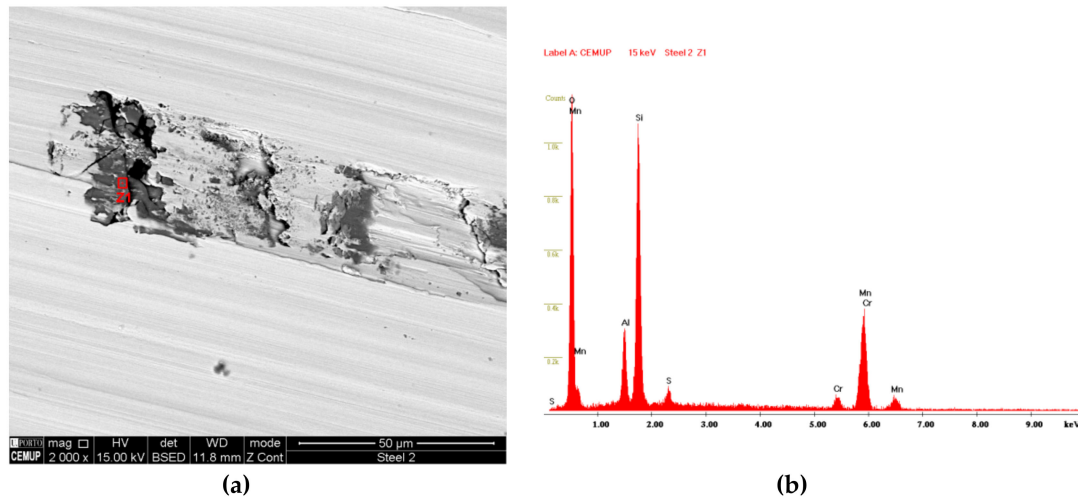


Figure 15. SEM images of small fragments retained in the chips. (a) SEM image of the hard fragment of the tool coating encased in the chip; (b) EDS confirmation of the fragment chemical composition.

As represented in Figure 15a, small fragments retained in the chips have also been detected. These chips were chemically analyzed by EDS (Figure 15b), being possible to identify that these are parts of insert coating, indicating that the applied coating is disintegrating.

4. Conclusions

It remains clear that DSS alloy is a material that has a very wide field of application when working conditions are truly challenging. Machining is an inescapable process for the manufacture of numerous parts, so there is a strong motivation to study the conditions that allow the machining of these alloys in the best way. The coatings used on carbide inserts is a proven path to increase tool lifespan regarding the previous studies already developed. This was a strong motivation for this work. Considering that there are PVD and CVD coatings of different materials that have been used in the machining of DSS alloys, the main objective was to compare the behavior of two different coatings, considering the same cutting conditions. Based on this objective and in the results obtained, it is possible to note that, for the conditions imposed by the tool manufacturer, the following were concluded:

- The substrate used in the CVD process has been shown to be more easily degradable than the one used for the PVD process. However, deterioration of the PH5740 carbide was more homogeneous (although more intense), not contributing significantly to the degradation of the surface quality of the machined parts;
- Regardless of the coating used in the cutting inserts, and considering the various parameters used to characterize the surface state of the machined surfaces, no significant differences were found regarding the three parameters used to evaluate the workpiece surface state;
- After deterioration of the coatings, both PVD and CVD, it is verified that the degradation of the substrate is accentuated, causing the disintegration of the carbide composite substrate in the area in contact with the workpiece. Thus, the longer the coating stays in operation on the surface of the insert, the lower the degradation of the substrate, and the better the surface quality of the obtained parts;
- Despite the greater degradation of the coatings and inserts with distance, for the selected cutting lengths there is no clear degradation of the surface quality of the machined parts;

- The incidents at the cutting edge of the inserts are very small, and should be essentially due to heterogeneities of the machined material;
- The worn area of the PVD deposited AlTiN coating was clearly lower than that presented by the TiCN/TiN/Al₂O₃ CVD coating, whereby the former shows to be more suitable for the machining of this DSS alloy under the selected cutting conditions;
- The flank face angle of 13° selected for the machining of this material does not appear to cause significant problems of deterioration of the cutting edge.

Thus, it is clear that under thinning conditions in the DSS machining it binds GX2CrNiMoN26-7-4, the coating of AlTiN carried out by PVD has an advantage over the coating of TiCN/TiN/Al₂O₃ made by CVD.

Author Contributions: Conceptualization, F.J.G.S. and H.M.L.; data curation: C.M.; formal analysis, F.J.G.S., H.M.L. and R.P.M.; investigation, F.J.G.S.; writing—original draft preparation, R.P.M. and F.J.G.S.; writing—review and editing, R.M.G.

Funding: This research received no external funding.

Acknowledgments: The authors would like to thank Daniel Figueiredo, from PALBIT company, due to providing the tools and material to be machined, as well as the sharing the images and data to Figures 1 and 2, and Table 1, Table 2, Table 3. The authors are also grateful for the help and professionalism of Rui Rocha from CEMUP in the SEM and EDS analyzes of worn tools. A special thanks is also given to the collaboration of Hernâni Lopes in the capture and analysis of the vibration diagrams obtained in the machining tests. Finally, the authors thank to ARSOPI, S.A. company due to the data provided for Table 4.

Conflicts of Interest: The authors declare no conflict of interest.

References

1. Manawi, Y.M.; Ihsanullah Samara, A.; Al-Ansari, T.; Atieh, M.A. A Review of carbon nanomaterials' synthesis via the chemical vapor deposition (CVD) Method. *Materials* **2018**, *11*, 822. [[CrossRef](#)] [[PubMed](#)]
2. Baptista, A.; Silva, F.J.G.; Porteiro, J.; Míguez, J.; Pinto, G. Sputtering physical vapour deposition (PVD) coatings: A critical review on process improvement and market trend demands. *Coatings* **2018**, *8*, 422. [[CrossRef](#)]
3. Pinto, G.; Silva, F.J.G.; Porteiro, J.; Míguez, J.; Baptista, A. Numerical simulation applied to PVD reactors: An overview. *Coatings* **2018**, *8*, 410. [[CrossRef](#)]
4. Martinho, R.P.; Silva, F.J.G.; Baptista, A.P.M. Wear behaviour of uncoated and diamond coated Si₃N₄ tools under severe turning conditions. *Wear* **2007**, *267*, 1417–1422. [[CrossRef](#)]
5. Martinho, R.P.; Silva, F.J.G.; Baptista, A.P.M. Cutting forces and wear analysis of Si₃N₄ diamond coated tools in high speed machining. *Vacuum* **2008**, *82*, 1415–1420. [[CrossRef](#)]
6. Silva, F.J.G.; Baptista, A.P.M.; Pereira, E.; Teixeira, V.; Fan, Q.H.; Fernandes, A.J.S.; Costa, F.M. Microwave plasma chemical vapour deposition diamond nucleation on ferrous substrates with Ti and Cr interlayers. *Diam. Relat. Mater.* **2002**, *11*, 1617–1622. [[CrossRef](#)]
7. Silva, F.J.G.; Fernandes, A.J.S.; Costa, F.M.; Baptista, A.P.M.; Pereira, E. A new interlayer approach for CVD diamond coating of steel substrates. *Diam. Relat. Mater.* **2004**, *13*, 833–928. [[CrossRef](#)]
8. Kuo, C.; Wang, C.; Ko, S. Wear behaviour of CVD diamond-coated tools in the drilling of woven CFRP composites. *Wear* **2018**, *398*, 1–12. [[CrossRef](#)]
9. Ramasubramanian, K.; Arunachalam, N.; Rao, M.S.R. Performance analysis of nano engineered diamond coated tools for machining of AA2124/SiCp composite material. *Procedia Manuf.* **2018**, *26*, 424–433. [[CrossRef](#)]
10. Silva, F.J.G.; Casais, R.C.B.; Martinho, R.P.; Baptista, A.P.M. Mechanical and tribological characterization of TiB₂ thin films. *J. Nanosci. Nanotechnol.* **2012**, *12*, 9187–9194. [[CrossRef](#)]
11. Silva, F.J.G.; Martinho, R.P.; Baptista, A.P.M. Characterization of laboratory and industrial CrN/CrCN/diamond-like carbon coatings. *Thin Solid Films* **2014**, *550*, 278–284. [[CrossRef](#)]
12. Silva, F.J.G.; Martinho, R.P.; Andrade, M.F.G.; Baptista, A.P.M.; Alexandre, R. Improving the wear resistance of moulds for the injection of glass fibre-reinforced plastics using PVD coatings: A comparative study. *Coatings* **2017**, *7*, 28. [[CrossRef](#)]

13. Boing, D.; de Oliveira, A.J.; Schroeter, R.B. Limiting conditions for application of PVD (TiAlN) and CVD (TiCN/Al₂O₃/TiN) coated cemented carbide grades in the turning of hardened steels. *Wear* **2018**, *416*, 54–61. [[CrossRef](#)]
14. Chinchanikar, S.; Choudhury, S.K. Wear behaviors of single-layer and multi-layer coated carbide inserts in high speed machining of hardened AISI 4340 steel. *J. Mech. Sci. Technol.* **2013**, *27*, 1451–1459. [[CrossRef](#)]
15. Chinchanikar, S.; Choudhury, S.K. Investigations on machinability aspects of hardened AISI 4340 steel at different levels of hardness using coated carbide tools. *Int. J. Refract. Met. Hard Mater.* **2013**, *38*, 124–133. [[CrossRef](#)]
16. Kene, A.P.; Orra, K.; Choudhury, S.K. Experimental investigation on tool wear behavior of multi-layered coated carbide inserts using various sensors in hard turning process. *IFAC Pap.* **2016**, *49*, 180–184. [[CrossRef](#)]
17. Navas, V.G.; Gonzalo, O.; Bengoetxea, I. Effect of cutting parameters in the surface residual stresses generated by turning in AISI 4340 steel. *Int. J. Mach. Tools Manuf.* **2012**, *61*, 48–57.
18. Chowdhury, M.S.L.; Chowdhury, S.; Yamamoto, K.; Beake, B.D.; Bose, B.; Elfizy, A.; Cavelli, D.; Dosbaeva, G.; Aramesh, M.; Fox-Rabinovich, G.S.; et al. Wear behaviour of coated carbide tools during machining of Ti6Al4V aerospace alloy associated with strong built up edge formation. *Surf. Coat. Technol.* **2017**, *313*, 319–327. [[CrossRef](#)]
19. Martinez, I.; Tanaka, R.; Yamane, Y.; Sekiya, K.; Yamada, K.; Yamada, S.; Hasegawa, M. Effect of coating layer loss on the wear rate change of coated carbide tools in turning process. *Precis. Eng.* **2017**, *50*, 1–7. [[CrossRef](#)]
20. Debnath, S.; Reddy, M.M.; Yi, Q.S. Influence of cutting fluid conditions and cutting parameters on surface roughness and tool wear in turning process using Taguchi method. *Measurement* **2016**, *78*, 111–119. [[CrossRef](#)]
21. Chail, G.; Kangas, P. Super and hyper duplex stainless steels: Structures, properties and applications. *Procedia Struct. Integr.* **2016**, *2*, 1755–1762. [[CrossRef](#)]
22. Iacoviello, F.; Di Cocco, V.; D'Agostino, L. Intergranular corrosion susceptibility analysis in austeno-ferritic (duplex) stainless steels. *Procedia Struct. Integr.* **2017**, *3*, 276–282. [[CrossRef](#)]
23. Paiva, J.M.F., Jr.; Amorim, F.J.; Soares, P.C., Jr.; Veldhuis, S.C. Tribological behavior of superduplex stainless steel against PVD hard coatings on cemented carbide. *Int. J. Adv. Manuf. Technol.* **2017**, *90*, 1649–1658. [[CrossRef](#)]
24. Luo, H.; Li, X.G.; Dong, C.F.; Xiao, K. Effect of solution treatment on pitting behavior of 2205 duplex stainless steel. *Arab. J. Chem.* **2017**, *10*, 90–94. [[CrossRef](#)]
25. Rajaguru, J.; Arunachalam, N. Coated tool performance in dry turning of super duplex stainless steel. *Procedia Manuf.* **2017**, *10*, 601–611. [[CrossRef](#)]
26. Tao, P.; Gong, J.; Wang, Y.; Jiang, Y.; Li, Y.; Cen, W. Characterization on stress-strain behavior of ferrite and austenite in a 2205 duplex stainless steel based on nanoindentation and finite element method. *Results Phys.* **2018**, *11*, 377–384. [[CrossRef](#)]
27. Cheng, X.; Wang, Y.; Li, X.; Dong, C. Interaction between austenite-ferrite phases on passive performance of 2205 duplex stainless steel. *J. Mater. Sci. Technol.* **2018**, *34*, 2140–2148. [[CrossRef](#)]
28. Zhou, N. Surface integrity of 2304 duplex stainless steel after different grinding operations. *J. Mater. Process. Technol.* **2016**, *229*, 294–304. [[CrossRef](#)]
29. Jebaraj, A.V.; Ajaykumar, L.; Deepak, C.R.; Aditya, K.V.V. Weldability, machinability and surfacing of commercial duplex stainless steel AISI 2205 for marine applications—A recent review. *J. Adv. Res.* **2017**, *8*, 183–199. [[CrossRef](#)]
30. Biksa, A.; Yamamoto, K.; Dosbaeva, G.; Veldhuis, S.C.; Fox-Rabinovich, G.S.; Elfizy, A.; Wagg, T.; Shuster, L.S. Wear behavior of adaptive nano-multilayered AlTiN/Me_xN PVD coatings during machining of aerospace alloys. *Tribol. Int.* **2013**, *43*, 1491–1499. [[CrossRef](#)]
31. Paro, J.; Hänninen, H.; Kauppinen, V. Tool wear and machinability of HIPed P/M and conventional cast duplex stainless steels. *Wear* **2001**, *249*, 279–284. [[CrossRef](#)]
32. Nomani, J.; Pramanik, A.; Hilditch, T.; Littlefair, G. Machinability study of first generation duplex (2205), second generation duplex (2507) and austenite stainless steel during drilling process. *Wear* **2013**, *304*, 20–28. [[CrossRef](#)]
33. Airao, J.; Chaudhary, B.; Bajpai, V.; Khanna, N. An experimental study of surface roughness variation in end milling of super duplex 2507 stainless steel. *Mater. Today Proc.* **2018**, *5*, 3682–3689. [[CrossRef](#)]
34. Selvaraj, D.P. Optimization of cutting force of duplex stainless steel in dry milling operation. *Mater. Today Proc.* **2017**, *4*, 11141–11147. [[CrossRef](#)]
35. Zhang, J.Z.; Chen, J.C.; Kirby, E.D. Surface roughness optimization in an end-milling operation using the Taguchi design method. *J. Mater. Process. Technol.* **2007**, *184*, 233–239. [[CrossRef](#)]

36. Sai, W.B.; Salah, N.B.; Lebrun, J.L. Influence of machining by finishing milling on surface characteristics. *Int. J. Mach. Tools Manuf.* **2001**, *41*, 443–450.
37. Gouveia, R.M.; Silva, F.J.G.; Reis, P.; Baptista, A.M.P. Machining duplex stainless steel: Comparative study regarding end mill coated tools. *Coatings* **2016**, *6*, 51. [[CrossRef](#)]
38. Krolczyk, G.M.; Nieslony, P.; Legutko, S. Determination of tool life and research wear during duplex stainless steel turning. *Arch. Civ. Mech. Eng.* **2014**, *15*, 347–354. [[CrossRef](#)]
39. Nunes, V.; Silva, F.J.G.; Andrade, M.F.; Alexandre, R.; Baptista, A.P.M. Increasing the lifespan of high-pressure die cast molds subjected to severe wear. *Surf. Coat. Technol.* **2017**, *332*, 319–331. [[CrossRef](#)]
40. Naskar, A.; Chattopadhyay, A.K. Investigation on flank wear mechanism of CVD and PVD hard coatings in high speed dry turning of low and high carbon steel. *Wear* **2018**, *396*, 98–106. [[CrossRef](#)]
41. Rупpi, S.; Larsson, A.; Flink, A. Nanoindentation hardness, texture and microstructure of $\alpha\text{Al}_2\text{O}_3$ and $\kappa\text{-Al}_2\text{O}_3$ coatings. *Thin Solid Films* **2008**, *516*, 5959–5966. [[CrossRef](#)]
42. *ISO 4288:1996 Geometrical Product Specifications (GPS)—Surface Texture: Profile Method—Rules and Procedures for the Assessment of Surface Texture*; International Organization for Standardization: Geneva, Switzerland, 1996.
43. Martinho, R.P.; Silva, F.J.G.; Martins, C.; Lopes, H. Comparative study of PVD and CVD cutting tools performance in milling of duplex stainless steel. *Int. J. Adv. Manuf. Technol.* **2019**, *102*, 2423–2439. [[CrossRef](#)]



© 2019 by the authors. Licensee MDPI, Basel, Switzerland. This article is an open access article distributed under the terms and conditions of the Creative Commons Attribution (CC BY) license (<http://creativecommons.org/licenses/by/4.0/>).